Effect of annealing conditions on the struct-optical properties of ZnFe$_{1.96}$La$_{0.04}$O$_4$ nanoparticles

R. Tholkappiyan[1*], Fathalla Hamed[1], K. Vishista[2]

[1]*Department of Physics, College of Science, United Arab Emirates University, Al Ain, United Arab Emirates*
[2]*Department of Physics, College of Engineering Guindy, Anna University, Chennai 600025, Tamilnadu, India*

[*]Corresponding author. Tel: (+97)1566130024; E-mail: thols2006@gmail.com

ABSTRACT

Lanthanum (La^{3+}) ion doped zinc ferrite nanoparticles were synthesized by combustion method using glycine as fuel. The as-synthesized ZnFe$_{1.96}$La$_{0.04}$O$_4$ nanoparticles were subjected to annealing temperature of 900 ^{o}C for time intervals of 2 h, 6 h, 12 h, 24 h and 48 h. The as-synthesized and annealed ZnFe$_{1.96}$La$_{0.04}$O$_4$ nanoparticles were characterized as a single phase with normal spinel structure. The surface morphology of these nanoparticles were found to be non–uniform and agglomerated with fine pores/voids. The induced strain and dislocation density were reduced with increasing annealing time which enhanced crystallinity and increased grain size. The values of optical band gap calculated from UV/Vis/NIR spectra of the as-synthesized and annealed ZnFe$_{1.96}$La$_{0.04}$O$_4$ nanoparticles were found to decrease with increasing annealing time. They range from 2.48 to 2.19 eV from the simple method and 2.42–2.12 eV for direct and 1.87–1.71 eV for indirect from Kubelka–Munk function method. The optical band gap in ZnFe$_{1.96}$La$_{0.04}$O$_4$ nanoparticles can be tuned as function of varying annealing time and it seems to correlate with induced strains in the nano-crystallites. Therefore, the tuning of optical band gap with just changing the heating treatment of ZnFe$_{1.96}$La$_{0.04}$O$_4$ nanoparticles may make them suitable photocatalysis. Copyright © 2016 VBRI Press.

Keywords: Spinel; zinc ferrite nanoparticles; temperature; structural; optical.

Introduction

Owing to their high surface area, nanocrystalline materials have displayed different properties than their bulk counterparts and they became the subject of interest for many material scientists over the past few decades. Magnetic materials like ferrite in the nano–regime could provide more advantages over bulk ferrites with remarkable changes in the physical, optical, electrical, thermal and magnetic properties. Applying these properties; nano-ferrites could be utilized in various recent practical applications such as high–density magnetic storage, ferrofluids, magnetic media, spintronics, microwave absorbers, magnetic refrigeration systems, repulsive suspension in levitated railway systems, sensors etc. **[1–5]**. On the basis of the crystal structure, cation distribution and magnetic ordering, ferrite materials can be classified into four different types—namely, spinels, hexa/hexagonal ferrites, garnets and orthoferrites. According to the distribution of cations either in tetrahedral and octahedral sites of spinel type–AB$_2$O$_4$ structure, where A and B are metal cations; spinels are classified into the following types: normal, inverse and random. Zinc ferrite is a kind of normal spinel structure with chemical formula Zn^{2+}Fe$_2$$^{3+}O_4$, where Zn and Fe refer to the metal ions that occupy in tetrahedral and octahedral sites. Nano–sized zinc ferrites show potentials that could be considered for applications in: data storage of information, drug delivery, electronic devices and medical diagnostics **[6, 7]**. In addition, the

spinel–structured zinc ferrite (ZnFe$_2$O$_4$) was established to be a promising material in detecting and reducing gases such as CO and CH$_4$ **[8, 9]**.

Generally, several synthesis methods such as wet–milling process **[10]**, sol–gel **[11]**, multi–step homogeneous non–aqueous solution synthesis method **[12]**, standard ceramic technique **[13]**, citrate precursor method **[14]**, ball-milling method [**15**], co–precipitation **[16]**, mechano-chemical reaction **[17]** etc. have been adopted for preparing the pure and metal–doped zinc ferrite nanoparticles as reported in literature. These methods have some advantages/disadvantages and limitations for preparing nanoparticles. Recently, much attention has turned towards a facile, flexible, reliable and cost effective method for preparing nanoparticles. One simple method is the auto–combustion technique. It is widely used for synthesizing the ferrite nanoparticles due to several advantages such as fast reaction rates, chemical homogeneity and high reactivity due to the efficient mixing and faster mass transfer of the reactants under low temperature medium. In addition, voids/porous morphology of nanomaterials was obtained. Based on practical applications, combustion method synthesized nanomaterials are more attractive in photocatalysis, filters due to the high surface area and porous morphology and are highly favorable for rapid faradaic electrode reactions in supercapacitor **[18]**.

In recent years, many researchers have become interested in the influence of rare earth elements substitution in

ferrites and then annealing on the structural, morphological and optical properties. For the substituted ferrites, changes in the structure, crystalline size, grain dimensions, cell parameters, chemical composition, morphology and band gaps which could be unitized in applications have been reported [19]. Recently, using a combustion method, a series of La–doped zinc ferrite with general formula of $ZnFe_{2-x}La_xO_4$ (x=0, 0.02, 0.04, 0.06) nanoparticles were synthesized from metal nitrates as starting source materials and glycine as fuel [20]. As a continuation of this work, we chose the $ZnFe_{1.96}La_{0.04}O_4$ samples and annealed them at a temperature of 900 °C over varying periods of time. As far as we know, apart from the synthesis of zinc ferrite nanoparticles, no investigations of the effects of annealing of $ZnFe_{1.96}La_{0.04}O_4$ nanoparticles have been reported. The objective of this study to is to report on the synthesis of $ZnFe_{1.96}La_{0.04}O_4$ nanoparticles by auto–combustion method using glycine as fuel. The novelty of this work is that it involves the effects of annealing at 900 °C over different time intervals on the structural, morphological and optical properties of $ZnFe_{1.96}La_{0.04}O_4$ nanoparticles. The annealed samples were characterized by X–ray diffractometry (XRD), scanning electron microscopy (SEM), Energy dispersive X–ray spectrometry (EDS), UV–Vis–NIR spectroscopy techniques, and Fourier transfer infrared spectroscopy (FTIR). The results are interpreted in terms of the influence of the annealing times on the structural, morphological and optical properties of the $ZnFe_{1.96}La_{0.04}O_4$ nano-ferrite material.

Experimental

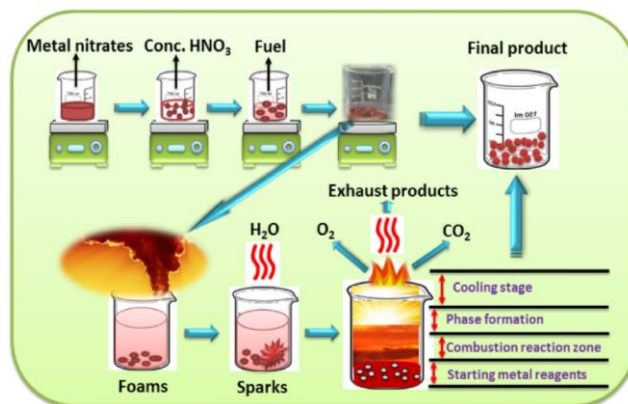### Materials

The starting precursors for this synthesis were metal nitrates such as purified zinc nitrate hexahydrate ($Zn(NO)_2 \cdot 6H_2O$, 96% purity, Merck), Iron (III) nitrate nonahydrate ($Fe(NO_3)_3 \cdot 9H_2O$, 98–100% purity, Alfa Aesar) and Lanthanum nitrate ($La(NO_3)_2 \cdot 6H_2O$, 99% purity, Alfa Aesar). Glycine ($C_2H_5NO_2$, 98.5% purity, Qualigens) was used as fuel. The starting precursors were of analytical grade without further purification.

Synthesis

First, the starting precursors were weighted and prepared into a solution containing a mixture of $Zn(NO)_2 \cdot 6H_2O$, $Fe(NO_3)_3 \cdot 9H_2O$ and $La(NO_3)_2 \cdot 6H_2O$ in 20 ml of distilled water under magnetic stirring for 30 minutes. In order to complete dissolving the solvents and initiate the combustion process, 5 ml of concentrated nitric acid (HNO_3) was added to the mixture and a clear aqueous solution resulted. The appropriate amount of fuel (glycine) was then introduced into the above solution and stirred for 20 min until complete dissolution occurred. To concentrate the above mentioned solution, heating at 80°C for 2 h under magnetic stirring was performed until excess free water had evaporated; a dark brown viscous gel was obtained. The heating temperature was then raised to 200°C which led to the auto ignition of the dried resin. At the beginning of combustion, it started to foam and produced sparks on the sides of the container/beaker. At the point of spontaneous combustion, it began to burn, and a dark brownish powder was obtained with the evolution of a large quantity of gases.

The time between the actual ignition and the end of the chemical reaction was less than 20 seconds. Finally, the as–synthesized products were removed and allowed to cool to room temperature; the resultant dried products were ground by hand with an agate mortar and pestle to a fine powder. The fine powder was calcined at 400 °C for 2 h. Different samples of the prepared powder were annealed at 900°C for different time intervals. All experiments were carried out in ambient conditions under air atmosphere. The schematic shows the preparation of $ZnFe_{1.96}La_{0.04}O_4$ nanopowders by combustion method [**Scheme 1**].

Scheme 1. Schematic represents the $ZnFe_{1.96}La_{0.04}O_4$ nanoparticles prepared by combustion method.

Characterizations

The X–ray diffraction patterns were recorded by SHIMADZU Lab X–XRD–6100 with CuKα line (λ=1.5418 Å). 2θ ranged from 10º to 80º with scanning rate of 0.02/min. The FTIR spectroscopy was carried out at room temperature using VARIAN 3100 FTIR, Excalibur series. The wavenumber was varied from 4000 to 400 cm^{-1}. Small amounts of the annealed powders were completely mixed with potassium bromide (KBr, BDH Chemicals Ltd, Poole, England) and pressed into 1 mm thick transparent discs. FTIR spectra were collected from these discs. Scanning Electron Microscopy (SEM) micrographs were taken by a JEOL JSM–6010LA operated at 20 keV accelerating voltage. Images were obtained in secondary electron imaging (SEI) mode and elemental analyses were performed with energy–dispersive X–ray spectroscopy (EDS). A Jasco V–670 spectrophotometers were used to measure the optical absorption spectra over a UV–Vis–NIR region in the diffuse reflectance mode. The light sources used are a deuterium (D2) lamp for the UV region and a halogen (WI) lamp for the VIS/NIR region. Small amounts of the annealed powders were completely dissolved into solvent to form a transparent solution. UV–Vis–NIR spectra were collected from these solutions.

Results and discussion

X–ray diffraction (XRD) studies

The phase identification of the synthesized powders was examined by X–ray diffraction. **Fig. 1** shows the powder XRD patterns of zinc lanthanum ferrite nanoparticles for the as–synthesized and annealed samples. The diffraction peaks in the XRD pattern for all samples were indexed to a

simple cubic structure with Fd–3m space symmetric group, according to the standard ICDD powder diffraction data (JCPDS # 22–1012).
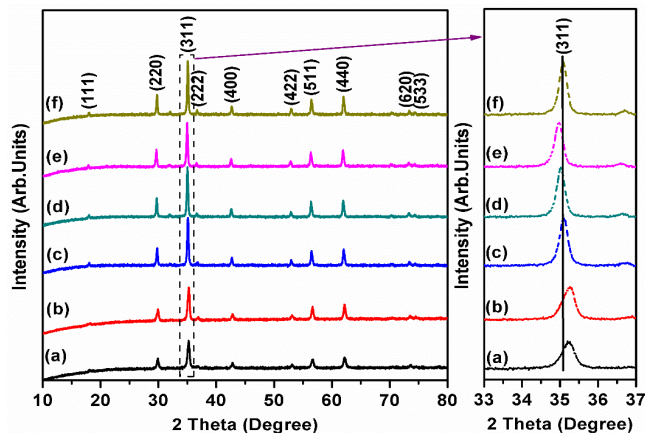

Fig. 1. Powder X-ray diffraction (XRD) pattern of $ZnFe_{1.96}La_{0.04}O_4$ nanoparticles at (a) as-synthesized, (b) 900°C for 2 h, (c) 900°C for 6 h, (d) 900°C for 12 h, (e) 900°C for 24 h and (f) 900°C for 48 h by combustion method.

No other extra/impurity diffraction peaks were detected in the powder XRD patterns. This indicates that the synthesized and annealed zinc lanthanum ferrite powders were of a single phase, further confirmations were obtained from FTIR studies. The broadening of diffraction peaks indicates the nanocrystalline nature of these ferrites. The intensity and sharpness of diffraction peaks increased with increasing annealing time interval; an indication of the growth of the average crystallite size. The average crystallite size (*d*) of the synthesized zinc lanthanum ferrite powders was calculated from Scherrer formula using the equation [20],

$$d = k\lambda/(\beta\cos\theta) \tag{1}$$

where, *d* is the average crystallite size, θ is the diffraction angle, λ (0.154 nm) is the wave length of X–ray beam, k is a constant (0.9 assuming nanoparticles are spherical in shape) and β is the full–width half maximum (FWHM). The average crystalline size estimated from diffraction line broadening is found to be in the range of 38–57 nm as listed in **Table 1**. It is seen that the average crystallite size increased with increasing annealing time at 900 ºC. This is due to the crystallization and coalescence of the smaller crystallites by solid–state diffusion where the system tends to lower its free energy by reducing the surface area [21].

The estimated value of average crystallite size for the as–synthesized powder was nearly in good agreement with the reported value of 35 nm for zinc ferrite prepared by mechanochemical reaction method and 38.2 nm for zinc ferrite powders prepared by wet–milling technique.

In an attempt to clarify structural analysis and calculate parameters like average crystallite size and lattice strain of the annealed samples, Williamson and Hall method (W–H) was suggested. The W–H method is usually an integral breadth method where both grain–size–dependent and strain–dependent broadening are fitted by a Lorentzian curve for all the peak width as a function of 2θ and FWHM (β). The Williamson–Hall equation can be expressed as [22],

$$\frac{K}{d} + \frac{4\varepsilon\sin\theta}{\lambda} = \frac{\beta\times\cos\theta}{\lambda} \tag{2}$$

Here ε is the lattice strain developed due to imperfection in crystal system and *K* is the shape factor.
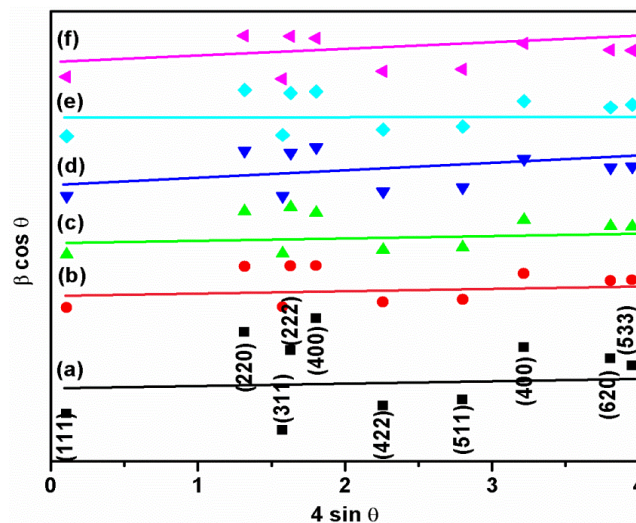

Fig. 2. Williamson and Hall method (W-H) plot of synthesized $ZnFe_{1.96}La_{0.04}O_4$ nanoparticles at (a) as-synthesized, (b) 900°C for 2 h, (c) 900°C for 6 h, (d) 900°C for 12 h, (e) 900°C for 24 h and (f) 900°C for 48 h by combustion method.

The W–H plots of $\beta\cos\theta$ versus $4\sin\theta$ for all the of diffraction peaks of the 900 ºC annealed zinc lanthanum ferrite nanoparticles are shown in **Fig. 2**. The W–H plot shows a straight line; by applying the best linear fit, the reciprocal of the intercept represents the average crystallite size and the slope gives the lattice strain. The W–H plots

Table 1. Average crystallite size (t) nm, X-Ray density (d_X), Surface Area (m²/g), Lattice Constant (a) (Å), Elastic strain (ε) (line⁻²m⁻⁴), Dislocation density (δ)((line/m²x10¹⁵) and band gap (eV) for the synthesized $ZnFe_{1.96}La_{0.04}O_4$ nanoparticles at different calcined time interval by combustion method.

Sample	t (nm)		X-Ray Density(d_X) g/cm³	Surface Area (S) (m²/g)	Lattice Constant (a) (Å)	Elastic strain (ε) (line⁻² m⁻⁴ x10⁻³)	Dislocation density (δ)((line/m²x10¹⁵)	Simple method	Band gap (eV)	
	Scherrer formula	W-H method							Kubelka–Munk function	
									Direct	Direct
ZF	38.46	29.08	5.37	38.37	8.452	80.62	11.82	2.48	2.42	1.87
900°C-2h	52.67	43.34	5.38	25.73	8.488	42.79	5.32	2.44	2.37	1.84
900°C-6h	52.74	41.93	5.33	26.84	8.480	37.04	5.68	2.41	2.30	1.79
900°C-12h	51.85	48.20	5.29	23.53	8.497	35.36	4.30	2.35	2.23	1.77
900°C-24h	54.99	51.71	5.27	22.01	8.510	31.96	3.73	2.24	2.18	1.73
900°C-48h	57.64	55.14	5.32	20.45	8.483	30.43	3.28	2.19	2.12	1.71

show lesser number of scatter points and good linear fits are established, this is an indication of the uniformity of the lattice strain. The values of average crystallite size and lattice strain obtained from H–W plots are listed in **Table 1**. However, in comparison with the Scherrer formula, the obtained average crystallite size from W–H equation are about 20% less for annealing times less than 6 h and nearly the same for annealing times more than 12 h. The later seem to happen as the strain gets lower. The positive value of lattice strain obtained from the slope of W–H plot indicates expansion. The strain is lowered as the annealing time is increased; this indicates that the structural distortion in zinc lanthanum ferrite samples pushes toward more relaxation.

The dislocation density (δ), defined as the length of dislocation lines per unit volume, it gives the number of defects or distortion in the crystal lattice. The dislocation density (δ) of the synthesized and annealed zinc lanthanum ferrite powders was estimated using the relation [23],

$$\delta = 1/d^2 \tag{3}$$

The values of dislocation density (δ) value obtained from the above equation are listed in **Table 1**. The table clearly shows that the value of dislocation density gets lower as the annealing time is increased. This in turn enhances the crystallinity of synthesized zinc lanthanum ferrite powders.

The lattice constants (a) for all the synthesized samples were calculated with the following equation [20],

$$a = [z^2 (h^2 + k^2 + l^2)]^{1/2} \tag{4}$$

where, z is the value of d–spacing of line and (hkl) is the Miller indices to each line in the XRD pattern. The values of lattice parameters of the synthesized zinc lanthanum ferrite powders annealed at different time intervals are summarized in **Table 1**. It was observed that there were little changes in the lattice parameters as the annealing time is increased. These changes in lattice parameters can be attributed to the change of crystallite size and variation in the ionic radii of La^{3+} and Fe^{3+} [24]. The ionic radii of La^{3+} (1.032 Å) is greater than that of Fe^{3+} (0.64 Å). La^{3+} ion with larger radius can enter into the crystal lattice of the synthesized zinc lanthanum ferrite powders and locate itself in the B–sublattice with adequate space [25]. Hence, the effect of annealing time on the B–sites of $ZnFe_{1.96}La_{0.04}O_4$ samples will cause the expansion of unit cell, resulting in the little changes in the lattice constant. In comparison, the calculated values of the lattice constants are in good agreement with the value of 8.44 Å reported in JCPDS, the value of 8.46 Å for zinc ferrite prepared via a co-precipitated un-milled method [26] and the value of 8.47 Å for fine powders of $ZnFe_2O_4$ (8.47 Å) synthesized by aerogel procedure [27].

The X–ray density (d_X) of the synthesized sample was calculated using the equation below [28].

$$d_X = 8M/N_A V \tag{5}$$

where, M is the molecular weight of the sample, V is the unit cell volume ($V = a^3$ for cubic) and N_A is the Avogadro's number ($N_A = 6.023 \times 10^{23}$/mol). The calculated values of

X–ray density of all synthesized samples are listed in **Table 1**. From the table, it is observed that X-ray density is nearly the same as the annealing time is increased. This is expected since there were very little changes in the lattice constant of the annealed samples.

The specific surface area (S) for all the synthesized samples were calculated with the help of X–ray density (dX) and average crystallite size (d) using the following equation [29].

$$S = 6/d_X(d) \tag{6}$$

The calculated values of specific surface area are listed in **Table 1**. It can be seen from the table that the specific surface area decreases with increasing annealing time interval. This may be attributed to the increase in crystallite size.
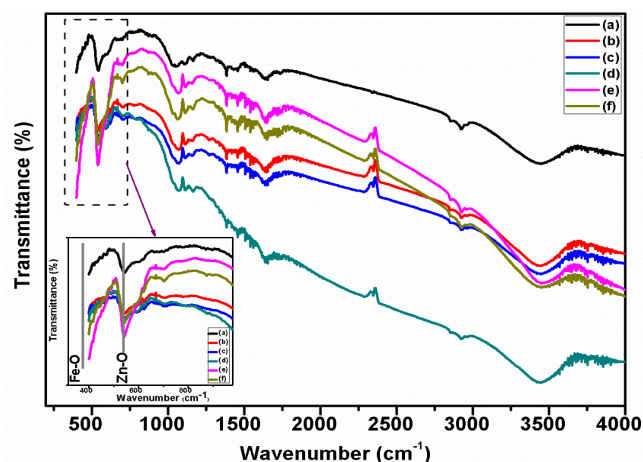

Fig. 3. FTIR spectrum of $ZnFe_{1.96}La_{0.04}O_4$ nanoparticles at (a) as-synthesized, (b) 900°C for 2 h, (c) 900°C for 6 h, (d) 900°C for 12 h, (e) 900°C for 24 h and (f) 900°C for 48 h by combustion method.

Fourier transfer infrared spectroscopy (FTIR) studies

The measured FTIR spectra of the annealed nano–crystalline $ZnFe_{1.96}La_{0.04}O_4$ particles are shown in **Fig. 3**. According to published reports [30], ferrite nanoparticles usually exhibit two bands between 400 and 600 cm^{-1} due to the stretching and vibrations of metal–O bond in tetrahedral and octahedral sites of spinel ferrites. In our annealed $ZnFe_{1.96}La_{0.04}O_4$ nanoparticles, these two bands occur at around ~410 and ~550 cm^{-1} corresponding to the stretching and vibrational modes of the octahedral Fe_{octa}–O and the tetrahedral Zn_{tetra}–O bond in the spinel zinc ferrites. The absorption band near 550 cm^{-1} is greater than 410 cm^{-1} due to the shorter length of tetrahedral bond than the octahedral [31]. The observed absorption band positions for the annealed $ZnFe_{1.96}La_{0.04}O_4$ nanoparticles are presented in **Table 2** as a function of annealing time interval.
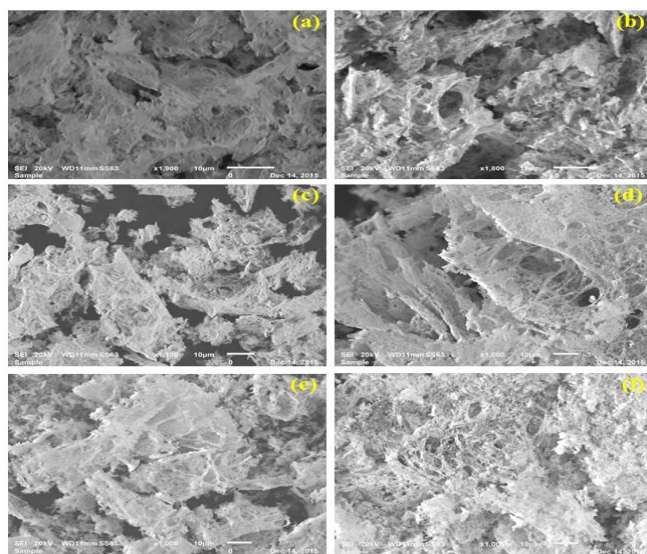
The two bands are shifted slightly upon increasing the annealing time interval and the band at ~ 550 cm^{-1} becomes broader as shown in insert **Fig. 3**. The broadening of the band indicates a cation vacancy in the lattice and a change in the lattice parameter of $ZnFe_{1.96}La_{0.04}O_4$ nanoparticles [32]. The vibrational frequency is directly proportional to the force constant (F_C) and the force constant can be calculated from the following relation [32],

Table 2: Peak assignment values of FTIR spectra for ZnFe$_{1.96}$La$_{0.04}$O$_4$ nanoparticles calcined at different time interval.

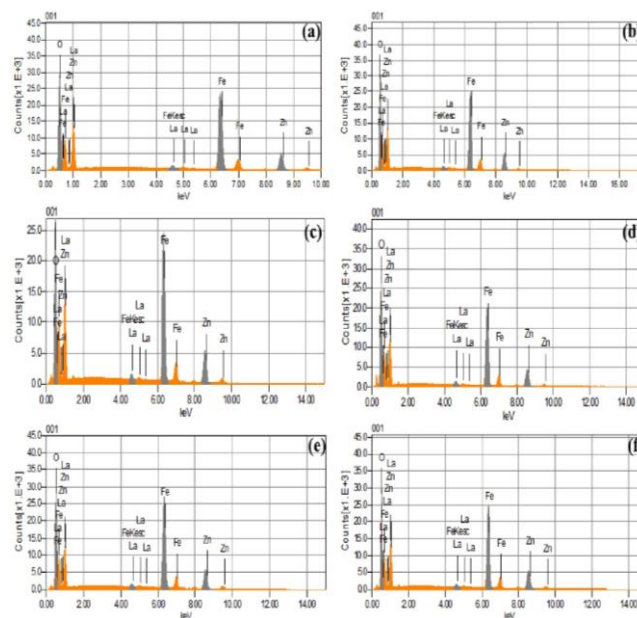| As-synthesized	900 °C-2 h	Wavenumber (cm^{-1}) 900 °C-6 h	900 °C-12 h	900 °C-24 h	900 °C-48 h	Peak assignments
410.67	415.35	409.67	406.81	404.15	403.67	Fe-O stretching vibration
546.87	537.01	551.80	541.94	535.18	556.73	Zn-O stretching and vibration
1059.23	1063.89	1074.58	1069.12	1053.21	1046.62	C–O stretching vibration
1343	1398	1351	1349	1377	1324	symmetric (COO) stretching vibration
1636	1642	1668	1654	1628	1649	asymmetric (COO) stretching vibration
2859	2868	2843	2891	2823	2846	C–H stretching mode
2926	2951	2973	2947	2933	2964	
3436	3467	3444	3499	3452	3487	O–H stretching vibration
		Force constant (F$_C$) (x10^5 dyne/cm)				
1.233	1.262	1.227	1.210	1.194	1.192	Fc$_{octa}$ (B-site)
2.187	2.109	2.227	2.148	2.095	2.267	Fc$_{tetra}$ (A-site)

$$F_C = 4\pi^2 c^2 \nu^2 m \qquad (7)$$

where, c is the speed of light = 2.99×10^{10} cm/sec, ν is the vibrational frequency of the octahedral and the tetrahedral sites and m is the reduced mass of the Fe^{3+} ions and the O^{2-} ions (m = ~2.061 x 10^{-23} g/mol). The calculated values of the force constant Fc$_{tetra}$ and Fc$_{octa}$ for the A and the B sites in the annealed ZnFe$_{1.96}$La$_{0.04}$O$_4$ nanoparticles are given in **Table 2**. It can be seen that both Fc$_{tetra}$ and Fc$_{octa}$ vary with different annealing time intervals. The bond observed at ~1050 cm^{-1} is due to the C–O stretching vibrations. The absorption bands around ~1353 and ~1640 cm^{-1} are assigned with the symmetric (COO) and asymmetric (COO) stretching vibrations of COO groups, these most likely came from minute quantities of carboxylate groups left from the glycine fuel during the auto combustion process. The two weak bands at around ~2850 and ~2950 cm^{-1} are assigned to the C–H stretching vibrations. The stretching vibrations at ~3460 cm^{-1} was associated with O–H (hydroxyl) groups, which may have resulted from water that was absorbed by the KBr used in the preparation of the thin transparent discs [33]. These FTIR studies confirmed the positions of the ions within the annealed ZnFe$_{1.96}$La$_{0.04}$O$_4$ nanoparticles, which were further supported by XRD measurements.

Fig. 4. SEM morphology of ZnFe$_{1.96}$La$_{0.04}$O$_4$ nanoparticles at (a) as-synthesized, (b) 900°C for 2 h, (c) 900°C for 6 h, (d) 900°C for 12 h, (e) 900°C for 24 h and (f) 900°C for 48 h.

Morphology studies

The synthesized ZnFe$_{1.96}$La$_{0.04}$O$_4$ nanoparticles were characterized by scanning electron microscope (SEM) to reveal their surface morphology. **Fig. 4 (a–f)** shows the SEM morphologies of the annealed lanthanum doped zinc ferrite nanoparticles. The formation of spongy and porous network structure was observed in all samples. These voids and pores are also present in the as synthesized sample. This porous formation took place during the combustion process where large amount of gaseous products such as nitrogen and carbon dioxide were produced. With annealing, these nanoparticles become non–uniform and agglomerated. This may be attributed to the interaction between the magnetic nanoparticles, in turn these particles grow to some extent to form larger particles at high temperatures [**34**].

Fig. 5. EDS analysis of ZnFe$_{1.96}$La$_{0.04}$O$_4$ nanoparticles at (a) as-synthesized, (b) 900°C for 2 h, (c) 900°C for 6 h, (d) 900°C for 12 h, (e) 900°C for 24 h and (f) 900°C for 48 h.

Energy dispersive x–ray spectroscopy (EDS) analysis

The elements present in the synthesized and annealed ZnFe$_{1.96}$La$_{0.04}$O$_4$ samples were analyzed by energy dispersive X–ray spectroscopy (EDS). **Fig. 5** shows the EDS spectra of the 900 °C annealed ZnFe$_{1.96}$La$_{0.04}$O$_4$ samples at time interval of 2 h, 6 h, 12 h, 24 h and 48 h.

The analysis of these EDS spectra indicates that the diffusion of lanthanum species within the zinc ferrites nanopowders spinel compound has taken place. No other elements were detected in the investigated samples which denote the quality of our samples as a single phase compound which was confirmed from XRD studies in **Fig. 1**. The elemental composition was determined from the EDS spectra to be close to the expected ratio of 1:1.96:0.04:4 for all the Zn, Fe, La and O atoms. In a previous study, we have confirmed the chemical composition of the synthesized $ZnFe_{2-x}La_xO_4$ (x=0, 0.02, 0.04, 0.06) nanoparticles from X–ray photoelectron spectroscopy (XPS) studies [**20**]. These results were considered in our EDS investigations. The integrity of our samples was verified by XRD, FTIR, SEM and EDS to form single phase $ZnFe_{1.96}La_{0.04}O_4$ spinel compounds.

UV/Vis/NIR spectroscopy studies

The energy band gap of synthesized and annealed zinc lanthanum ferrite nanoparticles was studied by UV/Vis/NIR spectroscopy. **Fig. 6** shows the optical reflectance spectra of the synthesized samples. The band gap energies of the annealed nano–crystalline $ZnFe_{1.96}La_{0.04}O_4$ powders were calculated from the wavelength value corresponding to the intersection point of the vertical and horizontal part of the spectrum, using the simple relation,

$$Eg = 1240/\lambda \qquad (8)$$

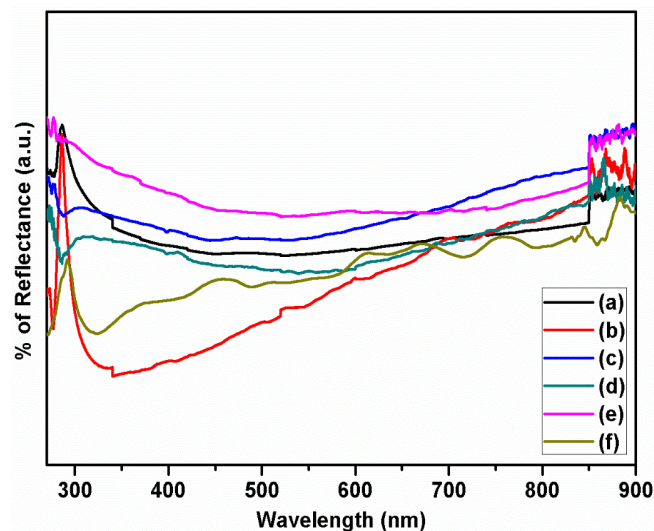whereas, Eg is the band gap energy (eV) and λ is the wavelength of spectrum in (nm).

Fig. 6. UV-Reflectance spectra for $ZnFe_{1.96}La_{0.04}O_4$ nanoparticles at (a) as-synthesized, (b) 900°C for 2 h, (c) 900°C for 6 h, (d) 900°C for 12 h, (e) 900°C for 24 h and (f) 900°C for 48 h by combustion method.

The calculated values of energy band gap from the above relation correspond to the absorption limit. These values are listed in **Table 1**. These results assigned the excitonic absorption behaviour of the annealed $ZnFe_{1.96}La_{0.04}O_4$ nanoparticles to be in the visible range 200–500 nm. This indicates that the electronic transitions are from the valence band to the conduction band (O–2p level into the Fe–3d level). This suggests that the synthesized $ZnFe_{1.96}La_{0.04}O_4$

nanoparticles are sensitive to visible light absorption and can be utilized in photocatalysts [35].

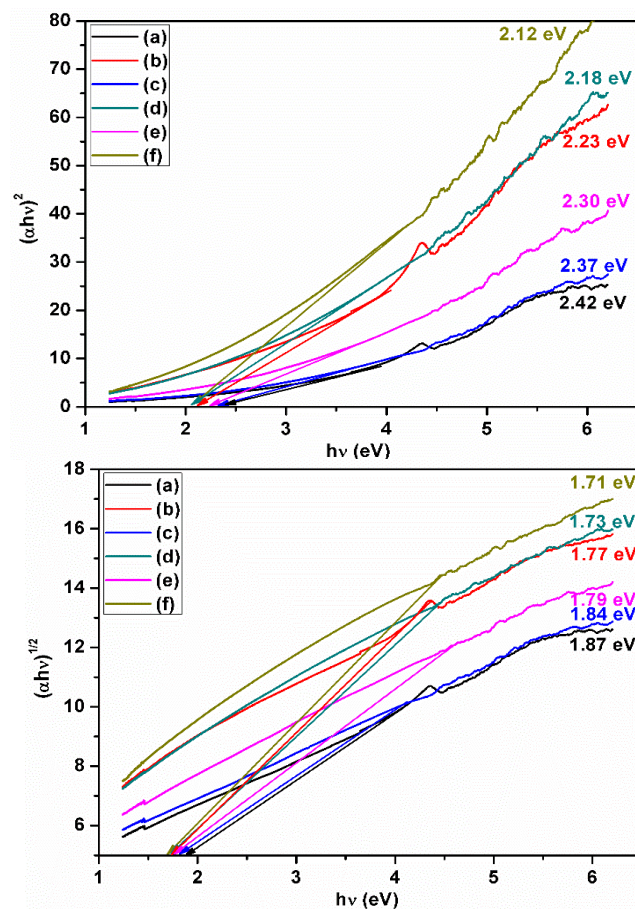**Fig. 7**. Direct band gap spectra (top) and Indirect band gap spectra (bottom) for $ZnFe_{1.96}La_{0.04}O_4$ nanoparticles at (a) as-synthesized, (b) 900°C for 2 h, (c) 900°C for 6 h, (d) 900°C for 12 h, (e) 900°C for 24 h and (f) 900°C for 48 h by combustion method.

In order to determine the precise value of optical band gap of synthesized $ZnFe_{1.96}La_{0.04}O_4$ nanoparticles, the reflectance spectra were converted to absorbance by using Kubelka–Munk function [**31–33**]:

$$\alpha=(1-R)^2/2R \qquad (9)$$

where, R and α is the reflectance and absorption coefficient. The band gap energy can be estimated from the absorption coefficient (α) using the Tauc equation [**36**],

$$(\alpha h\nu)=A(h\nu-E_g)^n \qquad (10)$$

where, $h\nu$ is the energy of the incident photon, A is a constant that depends on the transition probability and n is an index that characterizes to optical absorption process; n=1/2 for the direct allowed transition and n=2 for indirect allowed transition [**37**]. The optical band gap values of the annealed $ZnFe_{1.96}La_{0.04}O_4$ nanoparticles were obtained by extrapolating the linear portion of the plots of $(\alpha h\nu)^2$ vs. energy $h\nu$ (eV) for direct and $(\alpha h\nu)^{1/2}$ vs. energy $h\nu$ (eV) for indirect. The optical band gap (Eg) values obtained from the above calculations ranged from 2.42 to 2.12 eV for the direct and from 1.87 to 1.71 for the indirect. These values

are in good agreement with the reported value of 2.23 eV and 1.73 eV for direct and indirect band gaps of post–annealed $ZnFe_2O_4$ nanowires within anodic aluminum oxide templates [**38**] and the value of 1.90 eV (indirect) for $ZnFe_2O_4$ prepared by solid–state reaction method [**39**]. Our direct and indirect optical band gap values decreased with increasing the annealing time interval. This will enable the production of $ZnFe_{1.96}La_{0.04}O_4$

nanoparticles with different optical band gaps. Tuning the optical band gap with just changing the heating treatment may make these $ZnFe_{1.96}La_{0.04}O_4$ nanoparticles attractive for applications. Such a decrease in the $ZnFe_{1.96}La_{0.04}O_4$ optical band gap is in good agreement with the corresponding redshift seen in **Figs. 7** of absorption edge. It seems that the decrease in the optical band gap happens as the strains and dislocations are lowered. These stains and dislocations are increased as the nano-crystallite size decreased. This indicates that the optical band gap in $ZnFe_{1.96}La_{0.04}O_4$ nanoparticles are sensitive to the application of stresses which could be induced by surface tension. In addition to these interesting optical properties, $ZnFe_{1.96}La_{0.04}O_4$ nanoparticles show excellent magnetic response as we reported in a previous study where they can be easily separated from the dispersed solution by an external magnetic field [**35**].

Conclusion

In summary, $ZnFe_{1.96}La_{0.04}O_4$ nanoparticles were synthesized by combustion. The as-synthesized nanoparticles were annealed at 900 °C for varying periods of time. The as-synthesized and annealed $ZnFe_{1.96}La_{0.04}O_4$ nanoparticles were found to possess single phase $ZnFe_{1.96}La_{0.04}O_4$ with normal spinel structure. This was confirmed from XRD, EDS and FTIR studies. SEM studies revealed that the surface morphology of the as-synthesized and annealed $ZnFe_{1.96}La_{0.04}O_4$ nanoparticles is slightly agglomerated assembly of nanoparticles. The average crystallite size was found to increase with increasing annealing time while the surface area decreased. The positive strain and the dislocation density were lowered as the annealing time was increased. This has relaxed the strain induced structural distortion and enhanced the crystallinity. The calculated optical band gap (Eg) values from UV/Vis/NIR spectroscopy were found to decrease as the annealing time was increased. This seems to correlate with the relaxation of the strains. The tuning of the optical band gap in $ZnFe_{1.96}La_{0.04}O_4$ nanoparticles with changing the period of annealing was demonstrated. Thus, the tuning of optical band gap with just changing the heating treatment may make these $ZnFe_{1.96}La_{0.04}O_4$ nanoparticles attractive for applications in photocatalysis.
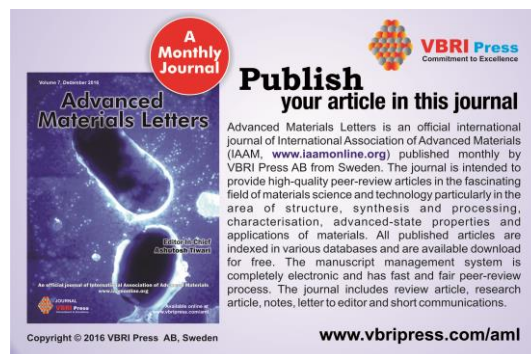
References

1. Mei Lin; Dongsheng Zhang; Junxing Huang; Jia Zhang; Wei Xiao; Hong Yu; Lixin Zhang; Jun Ye; *Nanotechnology*, **2013**, *24*, 255101.
   DOI: [10.1088/0957 4484/24/25/255101](10.1088/0957 4484/24/25/255101)

2. Lin, K.S.; Adhikari, A.K.; Tsai, Z.Y.; Chen, Y.P.; Chien, T.T.; Tsai, H.B; *Catal. Today*, **2011**, *174*, 88.
   DOI: 10.1016/j.cattod.2011.02.013

3. Srinivasan, G.; Taterenko, A.S.; Mathe, V.; Bichurin, M. I; *Eur. Phys. J. B*, **2009**, *71*, 371.
   DOI: 10.1140/epjb/e2009-00227-y

4. Jun, Y. W.; Seo, J. W.; Cheon, J; *Acc. Chem. Res.*, **2008**, *41*, 179.
   DOI: [10.1021/ar700121f.](10.1021/ar700121f.)

5. Banerjee, R., Katsenovich, Y., Lagos, L., McIintosh, M., Zhang, X., Li, C. Z; *Curr. Med. Chem*., **2010**, *17*, 3120.
   DOI: [10.2174/092986710791959765](10.2174/092986710791959765)

6. Lin, M., Huang, J., Sha, M; *J. Nanosci. Nanotechnol.*, **2014**, *14*, 792.
   DOI: [10.1166/jnn.2014.9135.](10.1166/jnn.2014.9135.)

7. Wang, G.; Su, X; *Analyst.*, **2011**, *136*, 1783.
   DOI: [10.1039/c1an15036g](10.1039/c1an15036g)

8. Lal, M.; Sharma, D.K.; Singh, M; *Ind. J. Pure Appl. Phys.*, **2005**, *43*, 291.

9. Suzuki, T.; Nagai, H.; Nohara, M.; Takagi, H; *J. Phys.: Condens. Matter*, **2007**, *19*, 145265.
   DOI: [10.1088/0953-8984/19/14/145265](10.1088/0953-8984/19/14/145265)

10. Sadan Ozcan; Burak Kaynar; Musa Mutlu Can; Tezer Firat; *Mater. Sci. Eng. B*, **2005**, *121* 278.
    DOI: 10.1016/j.mseb.2005.04.006

11. Rimi Sharma, Sonal Singhal, *Phys. B*, **2013**, *414*, 83.
    DOI: 10.1016/j.physb.2013.01.015

12. Tung, L. D.; Kolesnichenko, V.; Caruntu, G.; Caruntu, D.; Remond, Y.; Golub, V.O.; O'Connor, C.J.; Spinu, L; *Phys. B*, **2002**, *319*, 116.
    DOI: [10.1016/S0921-4526(02)01114-6](10.1016/S0921-4526(02)01114-6)

13. Ruiz, M. S.; Jacobo, S. E; *Phys. B*, **2012**, *407*, 3274.
    DOI: 10.1016/j.physb.2011.12.085

14. Ibetombi Soibam; Sumitra Phanjoubam; Sharma, H. B. ; Sarma, H. N. K.; Prakash, C; *Phys. B*, **2009**, *404,* 3839.
    DOI: 10.1016/j.physb.2009.07.107

15. Ghatak, S.; Chakraborty, G.; Sinha, M.; Pradhan, S. K.; Meikap, A. K; *Phys. B*, **2011**, *406,* 3261.
    DOI: 10.1016/j.physb.2011.05.036

16. Ren Ping; Zhang Junxi; Deng Huiyong; *J. Wuhan Univ. Technol. – Mater. Sci. Ed.*, **2009**, *24(6)*, 927.
    DOI: [10.1007/s11595-009-6927-y](10.1007/s11595-009-6927-y)

17. Balaz, P.; Calka, A.; Zorkovska, A.; Balaz, M; *Mater. Manuf. Process.*, **2013***, 28,* 343.
    DOI: [10.1080/10426914.2012.709294](10.1080/10426914.2012.709294)

18. Tholkappiyan, R.; Naveen, A. N.; Sumithra, S.; Vishista, K; *J. Mater. Sci.*, **2015**, *50 (17)*, 5833.
    DOI: [10.1007/s10853-015-9132-8](10.1007/s10853-015-9132-8)

19. Choodamani, C.; Nagabhushana, G. P.; Rudraswamy, B.; Chandrappa, G.T; *Mater. Lett.*, **2014**, *116*, 227–230.
    DOI: 10.1016/j.matlet.2013.11.024

20. Tholkappiyan, R.; Vishista, K; *Phys. B*, **2014**, *448*, 177.
    DOI: 10.1016/j.physb.2014.04.022

21. Amer, M. A.; Meaz, T.; Hashhash, A.; Attalah, S.; Fakhry, F; *J. Alloys Compd.*, **2015**, *649*, 712.
    DOI: 10.1016/j.jallcom.2015.07.157

22. Williamson, G. K.; Hall, W. H; *Acta Metall.*, **1953**, *1*, 22.
    DOI: [10.1016/0001-6160(53)90006-6](10.1016/0001-6160(53)90006-6)

23. Kathirvel, P.; Manoharan, D.; Mohan, S.M.; Kumar, S.; *J. Optocelectron. Biomed. Matter*, **2009**, *1*, 25.

24. Ishaque, M.; Islam, M. U.; Azhar Khan, M.; Rahman, I. Z.; Genson, A.; Hampshire, S; *Phys. B*, **2010**, *405,* 1532.
    DOI: 10.1016/j.physb.2009.12.035

25. Rao, A. D. P.; Ramesh, B.; Rao, P. R. M.; Raju, S. B; *J. Alloys Compd.*, **1999**, *282*, 268.
    DOI: [10.1016/S0925-8388(98)00823-8](10.1016/S0925-8388(98)00823-8)

26. Shenoy, S. D.; Joy, P. A.; Anantharaman, M. R; *J. Magn. Magn. Mater.*, **2004**, *269*, 217.
    DOI: [10.1016/S0304-8853(03)00596-1](10.1016/S0304-8853(03)00596-1)

27. Hamdeh, H. H.; Ho, J. C.; Oliver, S. A.; Willey, R. J.; Oliveri, G.; Busca, G; *J. Appl. Phys.*, **1997**, *81*, 1851.
    DOI: [10.1063/1.364068](10.1063/1.364068)

28. Kumar Mohit, Rout, S. K.; Parida, S.; Singh, G. P.; Sharma, S. K.; Pradhan, S. K.; Ill Won Kim, *Phys. B*, **2012**, *407*, 935.
    DOI: 10.1016/j.physb.2011.12.003

29. George, M.; John, A. M.; Nair, S. S.; Joy, P. A.; Anantharaman, M. R.; *J. Magn. Magn. Mater.*, **2006**, *302*, 190.
    DOI: 10.1016/j.jmmm.2005.08.029

30. Patil S.; Otarl S.; Mahajan V.; Patil M.; Patll A.; Soudagav N.; Patll B.; Sawant S; *Solid State. Comm.*, **1991**, *78*, 39.
    DOI: 10.1016/0038-1098(91)90805-6

31. Evans, B. J.; Hafner, S. S; *J. Phys. Chem.*, Solids **1968**, *29*, 1573.
    DOI: 10.1016/0022-3697(68)90100-5

32. Nasrazadani, S.; Raman, A; *Corros. Sci.*, **1993**, *34*, 1355.

33. Rahimi, M.; Kameli, P.; Ranjbar, M.; Hajihashemi, H.; Salamati, H; *J. Mater. Sci.*, **2013**, *48 (7)*, 2969.
    DOI: 10.1007/s10853-012-7074-y

34. Gharagozlou, M.; Bayati, R; *Superlattices Microstruct.*, **2015**, *78*, 190.
    DOI: 10.1016/j.spmi.2014.12.004

35. Pramod H Borse; Jae Young Kim; Jae Sung Lee; Kwon Taek Lim; Euh Duck Jeong; Jong Seong Bae; Jang-Hee Yoon; Seong Mi Yu; Hyun Gyu Kim; *J. Korean Phys. Soc.*, **2012**, *61*, 73.
    DOI: 10.3938/jkps.61.73

36. Tholkappiyan, R.; Vishista, K; *Sol. Energy*, **2014**, *106*, 118.
    DOI: 10.1016/j.solener.2014.02.003

37. Azim, O. A.; Abdel–Aziz, M. M.; Yahia, I. S; *Appl. Surf. Sci.*, **2009**, *255*, 4829.
    DOI: 10.1016/j.apsusc.2008.11.084

38. Gao, Daqiang; Shi, Zhenhua; Yan, Xu; Zhang, Jing; Yang, Guijin; Zhang, Jinlin; Wang, Xinhua; Xuel, Desheng; *Nanoscale Res. Lett.*, **2010**, *5*, 1289.
    DOI: 10.1007/s11671-010-9640-z

39. Jang, J. S.; Hong, S. J.; Lee, J. S.; *J. Korean Phys. Soc.*, **2009**, *54*, 204.